Lifetime improvement of EB-PVD 7YSZ TBCs by doping of Hf or Zr in NiCoCrAlY bond coats

Andrea Ebach-Stahl[1], Uwe Schulz[1], Radosław Swadźba[2], Ahmed Umar Munawar[1,3]

[1] DLR – German Aerospace Center, Institute of Materials Research, 51170 Cologne, Germany

[2] Łukasiewicz Research Network - Institute for Ferrous Metallurgy, Gliwice, Poland

[3]now at: School of Chemical and Materials Engineering, National University of Sciences and Technology, 44000, Islamabad, Pakistan

Contact Information:

Corresponding author:

Andrea Ebach-Stahl

DLR – German Aerospace Center

Institute of Materials Research

Linder Höhe

51170 Cologne, Germany

Email: andrea.ebach@dlr.de

Phone: +49 (0) 2203 601 2557

Abstract

Rare earth elements have a great positive influence on the oxidation behavior and thereby on the lifetime of TBC systems. A commonly used EB-PVD NiCoCrAlY bondcoat was doped by Hf and Zr in a range of 0.1-1 at.%. More than 3000 cycles were achieved by Hf-doping in a range of 0.15-0.6 at.% Hf which is a large improvement. Zr doped BCs provide high lifetimes of about 2800 cycles with a low doping content of 0.3 at.%. Microstructural changes, especially in the TGO, including formation of initially transient alumina, rare earth precipitates, and TGO evolution with time were examined in detail.

Keywords: A: NiCoCrAlY, A: EB-PVD TBC, A: Hf-doped bond coats, A: Zr-doped bond coats, C: RE-effect

Funding: The TEM work was performed in the Framework of the Research Project 2016/23/G/ST5/04128, funded by National Science Centre, Poland.

1. Introduction

NiCoCrAlY coatings on Nickel-based superalloys are frequently used in aero engines as well as gas turbine components. They form dense and continuous alumina scales during exposure to hot gases and protect thereby the base alloy. These coatings serve as overlay coatings as well as bond coats (BC) for ceramic thermal barrier coatings (TBC) [1]. TBCs, which usually consist of yttria partially stabilized zirconia (7YSZ), are well engineered in their properties such as a low thermal conductivity, tolerance against stresses and thermal shock. Especially TBCs fabricated by electron beam physical vapor deposition (EB-PVD) offer an advantage in mechanical properties in comparison to plasma sprayed TBCs, due to their inherent columnar microstructure [2-4]. It is generally accepted that the lifetime of TBCs depends on growth rate and adherence of the thermally grown oxide (TGO), which is linked to the type of BCs, especially composition and manufacturing, and also to the individual substrate alloy [5, 6]. The failure of EB-PVD TBC systems usually starts along the interface between TGO and BC [7-9]. Several investigations are engaged in lifetime extension of BC/TGO/TBC-systems. Minor amounts of reactive elements (RE) like Y, Hf, and Zr or combinations thereof affect the growth rate and adherence of the TGO, thereby changing the TBC lifetime [10-15]. Generally, a positive effect of Hf-doping on TBC lifetime is referred [10, 11]. In contrast, Zr doping is discussed controversially. Subanovic et al. [10] describe that co-doping of vacuum plasma-sprayed NiCoCrAl bond coats with 0.6 wt. % Zr (which equates to 0.3 at. %) and 0.6 wt. % Y extended the lifetime of EB-PVD TBCs, although the “overdoping” of the bond coat resulted in high TGO growth rates and crack formation within the TGO. Investigations by Song et al. [16] for additions of Zr on CoNiCrAlY bond coats resulted in an enhanced growth of the TGO and internal oxidation. In general, it is reported that RE elements have a positive influence on the oxidation behavior and the TBC lifetime due to several of factors that are still under debate. The effects include the suppression of the Al outward diffusion that changes the scale growth mechanism [17], increase in the interfacial strength [18], to getter detrimental sulfur from the

substrate alloy, to reduce void formation in or underneath the TGO, and to enhance TGO adhesion [19, 20].

For the TBC lifetime, an optimum RE content in bond coats seems to exist, which delivers the longest time until spallation of the top coat. This content seems to be individual for each bond coat – superalloy – RE combination and is only rudimentarily investigated. For bond coats on single crystals it is reported to be around 0.5at% Zr [21]. In our previous studies an improved TBC lifetime was found for both 7YSZ and Gd-zirconate (GZO) top coats on NiCoCrAlY bond coats doped with Hf. The Hf content was 0.15-0.3 at.% on 7YSZ [5] and 0.17 at.% on GZO coating systems [22].

The present study describes the influence of reactive elements on the microstructure and lifetime of NiCoCrAlY bond coats with a 7YSZ top coat. Due to the large influence of the doping elements and their concentration, this work examines bond coats with Hf and Zr addition with amounts from 0.1 to 1at.%. In particular a change in the TGO-morphology depending on the doping content was observed and compared to NiCoCrAlY-BCs without co-doping. With higher doping content the TGO was formed as a double layer, with the oxide of the doping element between Al_2O_3 and TBC after the coating process. The evolution of the TGO microstructure with time was examined in detail.

2. Experimental

Single crystal CMSX-4 cylinders with a diameter of 6mm and about 60mm length were used as substrate material. The coating manufacturing was performed by electron beam physical vapor deposition in a 150kW EB-PVD coater [22]. The samples were coated with a NiCoCrAlY bond coat doped with the reactive elements (RE) - Hf or Zr. The added content varied from 0.1 up to 1.0 at.% (see table 1). Note that for better comparison among each other all concentrations in this study are given in at.%.

In order to achieve the desired composition and to overcome the vapor pressure differences, the EB-PVD bond coat deposition was done with a two-crucible evaporation: NiCoCrAlY plus a second crucible for Hf or Zr evaporation, respectively. The evaporation was carried out by one electron beam gun operated in jumping beam mode. In order to achieve the desired RE contents, the evaporation rates of the RE crucibles were adjusted by changing the beam scan pattern sizes. The crucible arrangement was perpendicular to the rotation axis. In this way the required amount of Hf or Zr was added to the NiCoCrAlY coating with a good homogeneity along the sample length. The deposition time was around 30min with an average temperature of 1000°C. The doped bond coats were measured by X-Ray fluorescence analysis after the coating process for monitoring the composition and especially the required reactive element content. The bond coat thicknesses of all coating variants were about 90µm.

Before deposition of the ceramic top coat via EB-PVD, it is necessary to optimize the adhesion by peening and heat treatment at 1080°C for 4h under vacuum conditions. As top coat material 7 wt.% Yttria stabilized zirconia (7YSZ) was used with a composition of ZrO_2 – 6,8Y_2O_3 – 2,2HfO_2 in wt.%, measured by X-Ray fluorescence analysis. The TBC thickness was about 170µm. During all coating processes the samples were rotated on a planetary gearing holder.

After deposition the coating systems were tested cyclically at 1100°C in air. One cycle consisted of 50min heating and 10 min cooling down rapidly to nearly room temperature (about 60°C).

If a sample showed spallation of the TBC about 10mm or larger on the cylindrical surface, the sample was taken out of the test and declared as failure. Two samples per variant were tested.

Cross sections were made of representative samples (one per doping state) after TBC deposition (labeled here “as coated”) and after TBC failure. They were prepared by standard metallographic methods for microstructural examinations with a scanning electron microscopy (SEM; Zeiss Ultra 55). Compositions were measured by energy-dispersive X-Ray spectroscopy (EDS). Acceleration voltages of 3 keV were used for image acquisitions and 15 keV for EDS analysis.

The microstructure of the thermally grown oxide (TGO) as well as the metal-scale and TGO/YSZ interfaces was investigated using high resolution Scanning Transmission Electron Microscope (STEM) FEI TITAN 80-300 equipped with EDS detector by EDAX and an X-FEG operated at 300 kV. The microstructural imaging was performed using an atomic number sensitive (Z-contrast) High Angle Annular Dark Field (HAADF) as well as crystallographic orientation sensitive Annular Dark Field (ADF) detectors. Lamellas for STEM investigations were prepared by focused ion beam sectioning (FIB) in a FEI Helios Nanolab 600i FIB.

3. Results and discussion

3.1. Results of as coated systems

3.1.1. Hf-doped bond coats

These small modifications of the doping amounts caused noticeable changes in the bond coats: on the one hand, in comparison to the undoped reference NiCoCrAlY system and on the other hand it led to microstructural changes with increasing doping content.

Fig. 1 shows the as coated interface with TBC, TGO and BC of the reference sample. Typically for NiCoCrAlY bond coats, the TGO consists of a dense alumina layer with a thickness less than 1µm including an upper mixed zone of zirconia particles embedded in alumina. Yttria islands were seen locally between the TGO and 7YSZ. As commonly observed, underneath the yttria islands less or no zirconia particles are visible.

In addition, an Al depleted area exists underneath the alumina layer with a similar thickness to the TGO.

Contrary to the yttria islands between TGO and TBC, seen in the reference sample in Fig. 1, the Hf-doped system shows only an enrichment of hafnia above the TGO (Fig. 2). It starts to be visible in the variants having a 0.3 at.% Hf doping content or higher. Areas of a mixed zone were also found, but only in the regions where no hafnia islands were grown and a direct contact between alumina TGO and TBC exists. The mixed zone formation disappeared with increasing Hf addition. The 0.6Hf-BC possesses a nearly continuous hafnia-layer above the alumina TGO (Fig. 2b). In consequence, practically no areas of mixed zones could be detected. In all Hf-doped variants HfO_2 precipitates were seen below the TGO. All mentioned phases were verified with TEM analysis which is presented below.

The cross-sectional microstructure of the TGO formed on the 0.3Hf-BC during the coating deposition process was investigated by TEM and is shown in Fig. 3. As detailed in Fig. 3a, the TGO is around 650 nm thick and is characterized by the presence of aluminum oxides along with multiple nanometric inclusions, visible as medium gray in the Z-sensitive HAADF image

(Fig. 3a). Moreover, the interface between the TGO and 7YSZ as well as the bond coating is continuous and does not contain any porosities or voids. As observed in the SEM images, at the 7YSZ/TGO interface elongated white areas can be observed (Fig. 3b). Based on the electron diffraction pattern shown in Fig. 3c it can be concluded that it is HfO_2. Moreover, as shown in the elemental mappings in Fig. 3d-f hafnium is present only in those hafnia precipitates while the TGO underneath consists purely of Al and O. No additional hafnia enrichment, due to the Hf outward diffusion, was found within the 7YSZ top coat, although small amounts of Hf are present in the 7YSZ and were detected by EDS in SEM as common accompanying element. As can be observed in Fig. 3b, the areas where no hafnia is present between the YSZ top coat and the TGO contain multiple nanometric precipitates enriched in Zr and Y, as shown in elemental mappings of these elements (Fig. 3g, h).

Based on the STEM-HAADF image shown in Fig. 4a it can be observed that the precipitates present in the mixed zone of the TGO are around 10-20 nm in diameter and are evenly distributed within the alumina oxide scale. Moreover, no distinct grain boundaries of alumina could be observed in this region, therefore additional High Resolution TEM (HRTEM) imaging was performed (Fig. 4c). Based on that image a Fourier Transformation (FFT) was calculated (insert in Fig. 4c) representing the electron diffraction spots of the crystal planes present in the acquired HRTEM image. As shown in the FFT image spots corresponding to one of the transient alumina polymorphs, i.e. γ- or θ-Al_2O_3, along with tetragonal ZrO_2 were observed. It is noteworthy that the spots from particular crystal planes form concentric rings which are indicative of the presence of numerous nanometric sized grains. This result is in agreement with previous TEM investigations of the as-deposited TBCs on CVD aluminide [23] as well as MCrAlY bondcoatings [24].

3.1.2. Zr-doped bond coats

Similar to the Hf-doped samples, zirconia islands were seen between TGO and TBC at 0.7 at.% doping content and higher, which did not belong to the TBC due to their different microstructure (see Fig. 5). The nucleation of the initial columnar TBC growth can be clearly noticed above these islands. The formation of islands was not detectable at 0.3Zr-BC.

In general, a higher Al_2O_3 roughness was observed in Zr-doped BCs compared to NiCoCrAlY BC doped with Hf or the reference bond coating. With higher Zr-addition, an increasing Al_2O_3-roughness was noticed with a formation of oxide pegs reaching into the metallic bond coat. However, the interface between TBC and TGO is smooth and similar to other bond coat variants.

With a low Zr-doping the zirconia islands were mainly found in the cavities of the rough Al_2O_3-TGO. A nearly continuous zirconia layer was formed between TGO and TBC with a Zr doping content of 1 at.% (Fig. 5c). Moreover, a continuous mixed zone was observed in the TGO.

Contrary to the Hf doped bond coatings, no isolated zirconia precipitates were found within the metallic BC. The thickness of the Al_2O_3-TGO was found to be around 200nm, along with aluminum depleted zone within the bond coating with a comparable thickness to the Al_2O_3 layer.

3.1.3. TGO thickness in the as coated state

Based on the performed investigations, it has been found that the TGO structure and thickness after TBC deposition also depend on the doping content. The higher the RE content, the thicker and more continuous is the RE oxide between pure Al_2O_3 TGO and 7YSZ. The RE oxides start to form as localized islands for low RE contents and increase in number and size with rising dopant level, reaching a continuous RE-oxide layer at 0.3 at.% Hf and 1.0 at.% Zr. In comparison with the reference, the whole TGO thickness (Al_2O_3 + RE oxide) increases with higher RE contents (circle dotted lines in Fig. 6) in a similar way for both RE elements.

However, if only the pure Al_2O_3 TGO thickness is examined, its thickness decreases with increasing RE fraction. Within the measurement uncertainty, the thickness of the alumina layer for a given dopant level is slightly lower for the Zr-doped variant in comparison to the Hf-doped BC. This behavior correlates to the above mentioned assumption that during the vacuum annealing process RE elements diffuse outward and form islands or a rather nearly closed RE layer for high RE contents. During the vacuum annealing and the following pre-treatment, prior to the TBC deposition by EB-PVD, oxidation of these RE islands/layer takes place followed by the oxidation of Al. This RE oxide layer slows down the oxygen transport towards alumina (at least for high RE-concentrations), which results in a thinner Al_2O_3 TGO after TBC deposition process compared to the reference BC. Although differences in the oxygen transport through zirconia and hafnia need to be considered as well, the major differences in alumina thickness seem to arise from variations in TGO microstructure and phase composition. The Zr-doped BC developed a wavier microstructure and a thicker RE-oxide layer, that seem to have reacted in some areas with the 7YSZ TBC (see Fig. 5b and c) and resulted in a slightly thinner alumina layer underneath.

3.2. Discussion of as coated systems

It has been found that during the vacuum annealing process an outward diffusion of Y and Hf takes place. Since the reactive elements show a much higher oxygen affinity than all the other elements in the bond coat, the Y/Hf oxidize partially or completely due to the existence of residual oxygen in the vacuum atmosphere. The diffusion was found to take place mostly along grain boundaries in the bond coat. This behavior was observed in previous investigations and also described in other studies [25-27].

Depending on the RE-level in the bond coat, the TGO developed further during the TBC deposition process in oxygen containing atmosphere. It finally consists of a dense lower alumina layer and a local upper mixed zone consisting of zirconia particles embedded in

alumina, where a direct contact exists between the outer 7YSZ top coat and alumina. The Y/Hf-rich precipitates after the annealing process did not dissolve or react immediately with the alumina, but remain as oxidized particles on top of the TGO. These islands seem to serve as a diffusion barrier, so that a mixed zone was formed only in the vicinity of the islands. Due to the small size of the yttria-islands, this behavior is only seen locally in the reference sample.

In the Hf-doped bond coats the coverage by hafnia depends on the Hf content. For Hf levels of 0.3 at.%, or lower, the hafnia is represented as islands similar to yttria in the reference BC. For Hf levels of 0.5 at.% and higher a more or less complete coverage of the TGO by hafnia was found. Those highly doped variants also showed internal oxidation of Hf that forms HfO_2 predominantly along grain boundaries of the bond coat. The number of internally formed hafnia increases with raising Hf dopant level. The dependence on the doping content to the TGO thicknesses will be discussed later in detail in the chapter "TGO thickness in the as coated state".

The effect of the Hf islands can be explained by the oxygen diffusion coefficient D_0. Investigations of Vos et. al. determined the coefficient $D_0 = 1 \times 10^{-13}$ cm²/s in hafnia at 1100°C [28]. D_0 in zirconia is five orders of magnitude higher [29], while the coefficient in alumina is distinctively smaller ($D_0 = 1 \times 10^{-21}$ cm²/s at 1400°C [30]). The oxygen inward diffusion is clearly decelerated by the presence of hafnia on top of the TGO. In addition the formation of zirconia particles originating from the TBC deposition process was also completely suppressed within the TGO in those areas. TEM investigations confirmed that no zirconia particles could be found in the TGO directly underneath these hafnia areas, however they are found only in the regions next to these hafnia islands, where a direct contact between Al_2O_3 and TBC exists. Interestingly, no hafnia was detected in the mixed zone area. Apparently, the outward diffusion of Hf occurs mainly during the vacuum annealing.

The occurence of the mixed Al_2O_3 / ZrO_2 zone has been reported in previous research works [5, 31, 32], and was suggested to form upon deposition of the YSZ top simultaneously to the growth of transient alumina polymorphs by outward cationic Al^{3+} diffusion. It is suggested that the fine YSZ particles are embedded in the growing TGO during the EB-PVD process. Contrary to this, when the outer ceramic top coating is deposited on already formed (pre-oxidized) substrate covered with α-Al_2O_3, no mixed zone is observed [32-34].

This is also found for the present Hf- and Zr doped BCs where an outward RE diffusion took place during vacuum annealing. The RE will eventually oxidize during the pre-treatment prior to TBC deposition, like Y in the reference samples. While hafnia forms in a similar manner as yttria, the formed zirconia islands have a different microstructure. In addition, the formed mixed zone differed in microstructure for Zr-doped BCs from that of the Y or Hf-doped BC. It seems that the 7YSZ particles were not embedded in the growing alumina TGO, while the zirconia layer that was formed during vacuum annealing was incorporated into the TGO, forming a mixed zone. The increasing Al_2O_3 roughness can be explained by the fast diffusion of oxygen cations in zirconia. Presumably areas with higher zirconium content after annealing oxidized faster and formed the oxide pegs to be seen in Fig. 5c.

For both studied dopant additions, islands of the oxidized Hf or Zr were found above the TGO after TBC deposition process. Both Hf- and Zr-doped bond coatings formed a mixed zone area composed of Al_2O_3 and ZrO_2 particles from the TBC next to these islands. Due to their role as a diffusion barrier, no particles of the 7YSZ were found in the TGO underneath the hafnia or zirconia islands. In the Hf-doped variant, only pure Al_2O_3 was found, which was proved by the TEM-investigations, shown in Fig. 3. The effect of the mixed zone formation is more pronounced of the Hf-doped variant comparable to the Zr-doped ones. With increasing the doping content, a nearly continuous oxidized layer of the oxidized doping element was found and the formation of the mixed zone with TBC particles embedded in Al_2O_3 was inhibited.

This behavior of a diffusion barrier and local formation of mixed zone is also described by W. Braue et al. [26], who investigated a similar behavior of yttrium in the NiCoCrAlY coatings, which were also pretreated by vacuum annealing before TBC deposition. Fig. 7 schematically represents the diffusion processes and formation of the mixed zone upon TBC deposition which is validated in the present study for Hf and Zr-doping. As commonly observed in those bond coats, alumina grows mostly inwardly during oxidation.

Interestingly, the yttria islands, that were observed on top of the alumina scale in the reference sample (Fig. 1) after the vacuum annealing process, were not found on the Zr- or Hf-doped bond coatings, although all the studied systems contain around 0.1-0.2 at. % of Y, which is similar to the Y content in the reference system. Instead, in both doped systems exclusively zirconia or hafnia was found to be present on top of alumina. One possible explanation for this phenomenon could be a higher growth rate of either Zr or Hf oxides compared to Y oxides and their competition during the vacuum annealing process. Additionally, in comparison to the observations at Y/Hf doped NiCoCrAl free-standing coatings of Subanovic et al. [35], a second explanation for the preferential hafnia and zirconia formation is a faster diffusion of Hf and Zr in the BC.

3.3. Condition after 1100°C test

3.3.1. Lifetime investigations

The end of lifetime criterion of the coatings was defined by a spallation of an area of 10mm or more in length. For 7YSZ on NiCoCrAlY bond coats, the complete failure generally takes place during one cooling event of the particular lifetime limiting cycle. But the most RE-doped BC-TBC systems showed another behavior, in particular the variants with a high lifetime. Here a slowly progressing failure behavior was observed caused by the excellent adhesion of the coatings. TBC cracks were seen first most of the time, which were visible during the moving out of the furnace due to the local higher cooling rates. The coating spallation started much later after accumulation of more cycles. This TBC spallation occurred only in small dots, which did

not achieve the end of lifetime criterion at first but grew slowly in size during the following cycles. This special TBC spallation behavior that is different from the usual spallation of larger TBC areas is shown in Fig. 8. For some samples, mostly the high Hf-doped coatings, it was necessary to deviate slightly from the pristine failure criterion. After long testing times, the lengths of the spallation dots were summed up and the test was terminated once a critical total failure area was achieved. This decision was applied since in real engine situations this kind of cracks and spallation would lead to further damage and the TBCs would be declared as failed.

In Fig. 8, it is visible that most doped bond coats result in a large increase in TBC lifetime up to 2500 cycles and higher. The dependency of lifetimes on the doping content behaves contrary for both doping elements. The Hf-doped bond coatings show a longer lifetime with higher Hf content, while the lifetime of the Zr-doped ones decreases with increasing doping content. In general, a great improvement is evident with an additional RE doping of NiCoCrAlY BC, while the reference that was established on a high number of samples only reached a lifetime of 311 cycles at 1100°C [5]. Additionally, the scattering within each variant is very low, so that the testing of only two samples was possible, although random effects of the typically statistical failure of TBCs may have been involved here as well.

Fig. 9 shows the lifetime as a function of the RE doping content. The curve of Hf-doped BCs increases rapidly until a content of 0.15 at.% (circle dotted green line, Fig. 9). Then the slope decreases and seems to saturate. Generally, there exists a relatively wide range of Hf doping content (0.15-0.6 at.%) which leads to lifetimes above 3000 cycles.

This wide Hf addition range providing longer lifetimes can also be confirmed by former investigations on NiCoCrAlY-SiHf bond coats [5], where with a Hf content of about 0.3 at.% a lifetime of nearly 4700 cycles was achieved. However, it is to be mentioned that this lifetime was determined on the strict spallation criterion of 10mm in length, described in the first passage of this chapter. By applying the more appropriate and more severe failure criterion here, the lifetime shifted into the present lifetime range of Hf additions without Si. This implies

that the positive influence of Hf doping content on the lifetime is significantly higher than the influence of Si additions.

The lifetime curve of Zr-doped BC seems to show a different behavior in comparison to Hf doping. High dopant contents, e.g. 1.0 at.% of Zr, have no influence on the lifetime compared to the reference BC. Interestingly, the highest lifetime observed in the current study was achieved by the bond coating doped with 0.3 at.% of Zr. It can only be speculated here that higher Hf doping contents than 0.6 at.% may result in a decreasing lifetime caused by overdoping. In this case, the general trends in lifetime would be similar to Zr-doping with a shifted maximum, while the doping range with lifetime improvement is wider for Hf doping.

3.3.2. Microstructure of Hf-doped bond coats

The microstructure of the tested Hf-doped BCs is represented in Fig. 10. Distinct differences can be seen with increasing Hf content, mainly in the upper region of the TGO. As shown in Fig. 10a, a mixed zone underneath the TBC (Al_2O_3 + ZrO_2 particles) was formed in the 0.15Hf-BC. Directly below the mixed zone small dots with a slightly light-colored contrast compared to the ZrO_2 particles occur locally, which most likely consist of hafnia. Pores also exist in the region of the mixed zone. Underneath the mixed zone a dense TGO of Al_2O_3 with localized grains that are rich in Ni and Cr and also hafnia particles are visible.

The TGO thicknesses varied from 16-25µm. Unfortunately, the TGO data was not consistent enough and showed substantial scattering due to the waviness and roughness of the interface between TGO and bondcoat. In cross sections several gaps and cracks in various locations were found in the vicinity of the TGO. Moreover, it cannot be excluded that some cracks have formed during metallographic preparation, although great care has been applied to avoid any damage to the TGO during cutting and grinding.

With increasing Hf content the formation of the mixed zone was suppressed. As can be seen at the as coated state in Fig. 2b a nearly continuous hafnia layer was already formed after TBC deposition. This layer shows a high stability against diffusion or reaction with other phases and exists still after about 3000 cycles (Fig. 10b). An Hf outward diffusion into the TBC could be excluded via EDS measurements.

The high stability of hafnia particles is also verified in the marked “area with hafnia particles” in Fig. 10b. These hafnia particles were already seen below the TGO in the as coated state (Fig. 2). After testing, these precipitates were embedded in the Al_2O_3 matrix. Below this area the brighter gray grains (most likely spinel) and small hafnia dots were also observed in the Al_2O_3 TGO. The hafnia particles are smaller in the 0.15Hf-BC than in the 0.3Hf-BC variant, similarly to the as coated condition. This indicates a high stability and only a moderate grain growth and coarsening of those particles within alumina during prolonged oxidation. Pores could only be seen in the upper part of Al_2O_3 directly underneath the hafnia layer.

The microstructure of the 7YSZ/TGO interface formed on the Hf-doped bond coating (0.3 at.%) during furnace cyclic testing was further analyzed by TEM and is shown in ADF and HAADF images in Fig. 11a,b. In the HAADF image shown in Fig. 11a it is visible that the hafnia precipitates that formed during the initial growth of the TGO are still present between it and the 7YSZ top coat. It is clearly illustrated in the distribution mapping of hafnium shown in Fig. 11c. Additionally, no segregation of hafnium was found in the 7YSZ top coating. Moreover, sintering of the YSZ top coating is visible compared to the as-deposited state (Fig. 3a). As seen in SEM, underneath the hafnia layer considerable porosity can be observed in the TGO in addition to bright gray and dark gray areas. The elemental mappings of Ni and Al, shown in Fig. 11d and e respectively, indicate that the bright gray regions contain both these elements in addition to oxygen (Fig. 11f) while the dark gray regions consist of Al and O. Based on the electron diffraction patterns it is clear that the former regions consist of $NiAl_2O_4$ spinel, while the latter are α-Al_2O_3. The distribution mappings of Y and Zr (Fig. 11g, h) indicate these

elements are present only within the 7YSZ top coat. The crystallographic orientation sensitive ADF detector provided information on the grain structure in the analyzed area of the TGO. As shown in Fig. 11b, both the spinel as well as alumina regions are characterized by an equiaxed microstructure. This is contrary to the observed nanocrystalline structure of the transient θ-alumina in the initially grown TGO. The alumina grains observed after the cyclic oxidation test are around 100-300 nm in diameter and of globular shape. In addition to the results of phase identification within the TGO in the as-deposited condition, this observation further proves that the alumina transformed from nanocrystalline grains of its transient polymorphs (either γ or θ) to the stable α-Al_2O_3 with much larger equiaxed grains. These results are similar to our previous findings (Braue et al. [25, 26]) and agree well with the investigations by Quadakkers et. al. [36]. As evidenced by the SEM investigations shown in Fig. 10, the TGO formed during the cyclic oxidation test on all the studied bond coats is mostly composed of alumina with some grains rich in nickel, chromium and cobalt. In order to study in more detail the microstructure of the TGO formed on the bond coating modified with 0.3 at% Hf, additional STEM investigations were performed in the middle region of the TGO. The STEM-HAADF images shown in Fig. 12 and 13 correspond to the part of the TGO that formed by oxidation reaction, as opposed to the microstructure shown in Fig. 11 where most of it formed by initial transient oxides formation and subsequent transformation. As shown in Fig. 12a the TGO consists of a mixture of alumina, visible as dark gray, along with light gray grains containing mostly Ni, Al and O, as shown in the elemental mapping of these elements (Fig. 12) and also white particles containing Hf and O. Using electron diffraction, it was possible to identify the presence of HfO_2 and $NiAl_2O_4$ phases which were marked in Fig. 12b. Moreover, the elemental mappings of Co and Cr indicate that these elements are also segregated to the spinel phase. Moreover, Zr was found to segregate to the HfO_2 grains. In addition to the major constituents of the TGO, additional segregation of Y was found on the grain boundaries between the alumina, spinel and hafnia. These nanometric particles with size of around 50 nm were identified as Y_2O_3 by

electron diffraction (Fig. 12). Since the HAADF detector is sensitive to the atomic number of the elements (Z-contrast), it is possible to differentiate the chemical segregation phenomena in the analyzed regions. As shown in Fig. 12, the grain boundaries between alumina grains appear brighter compared to the surrounding phases which indicates the presence of additional elements. Further investigations shown in Fig. 13 reveal the formation of alumina grains doped with additional elements along with formation of Hf-rich precipitates (HfO_2 in this case). As evidenced using STEM-EDS elemental mapping in the area shown in Fig. 13b it was possible to reveal the presence of reactive elements segregation to the grain boundaries, such as Hf, Y and Zr, along with Ni segregation.

3.3.3. Microstructure of Zr-doped bond coats

Zr-doped NiCoCrAlY BCs show a completely different TGO microstructure compared to BCs with Hf. The Zr-islands and the mixed zone seen in the as coated state (Fig. 5) disappeared completely during the cyclic oxidation test.

A massive spinel formation was seen at high Zr contents from 0.7 at.% and higher, mostly in the upper region of the TGO (Fig. 14). Presumably, this spinel formation is the reason that no improvement in lifetime was seen by higher Zr additions. The reduction of the Zr content reduced this spinel formation and a distinct lifetime prolongation was observed. BCs with 0.3Zr formed a dense Al_2O_3 layer. Only small spinel precipitates were embedded in the alumina. The TGO-thicknesses varied from 17 to 25µm.

3.4. Discussion of condition after 1100°C test

The RE islands observed in the as coated state and after the cyclic oxidation testing show a high stability and their behavior as a diffusion barrier against elements diffusing from the TBC into the TGO was not lost and, therefore, the mixed zone formation was fully suppressed. The formation and the influence of the mixed zone on the lifetime of TBCs are discussed in literature

in detail with diverse arguments and effects [24-26, 37, 38]. Both lifetime prolonging and shortening effects were found. A positive or negative effect of the mixed zone could not be finally clarified in those studies. In this study, longer lifetimes are accompanied by suppression of the mixed zone, but it is not clear whether the lifetime is enhanced by the presence of the continuous hafnia layer between TGO and TBC or by the absence of the mixed zone, or by both effects.

The visible segregation of reactive elements to the grain boundaries of growing alumina scales (seen Fig. 13) has been the subject of numerous research works [17, 33, 39-42] and reviews [19, 20, 43]. Since both Zr and Y are present in the ceramic YSZ top coating, their origin in the grain boundaries of alumina could be argued. However, it is generally accepted that these elements diffuse outward from the substrate or bond coat to the gas-scale interface in the oxygen potential gradient across the growing TGO [44]. In addition, the studied bond coat is doped with both Y and Hf (NiCoCrAlY-0.3Hf). The source of Zr could also be a minor amount of this element in either the bond coat or even the substrate alloy. It was shown in previous studies that this element could be found in oxide scales formed on a bare 2nd generation SX superalloy [45]. Moreover, the formation of secondary oxides, such as HfO_2 or Y_2O_3, in the grain boundaries of alumina can result from the supersaturation of these elements in the present bond coats. Additionally, the evidenced segregation of Ni can suggest the outward diffusion of this element which in turn may facilitate the growth of the spinel phase within the TGO.

Based on TEM observation it is suggested that the formation of the equiaxed grains occurred upon the transformation from the transient γ- or θ- to the stable α-Al_2O_3 [46]. Moreover, the voids found within the upper part of the TGO were most likely formed due to the volumetric changes accompanying this transformation [47, 48].

Research works on sputtered NiAlCr-Zr bond coats with a Zr content of 0.7at.% or lower of Muñoz Saldaña et al. [49] also did not reveal spinel formation, although the composition there deviated from the current BCs with an higher Al content of approximately 30 at.% and a distinct

lower Cr fraction of about 5 at.%. The current results indicate that a critical Zr content for increasing spinel formation exists, depending on the overall composition of the bond coat. In general, the formation of spinel in the alumina TGO was not found to be detrimental for TBC life which is in good agreement to our previous research [5]. Spinel formation is an effect that is seen only for long oxidation times since its formation in the TGO is slow. It is also very likely that the metallic regions between alumina oxide pegs/stringers get entrapped by the oxide, and in a later stage oxidize to spinel.

Finally, the role of the TGO pegs that reach into the bond coat and form a rough interface between BC and TGO needs to be discussed. It is believed that they are positive for TBC life since they increase the energy needed to drive a crack along that interface, simply because the crack has either to change the direction very often or is has to bridge the metal in between the oxide stringers. The current data support this argument in principle, although the 0.7 at% Zr possess pegs but did not increase TBC life. This indicates the plurality of factors that finally rule the lifetime of a TBC system.

Overall, Hf-doping seems to be more effective than Zr-doping for TBC lifetime when similar atomic concentrations in the bond coat are compared. It is believed that besides different reactivity and oxygen transport properties the differences are mainly caused by changes in the TGO microstructure such as spinel formation, roughness of the oxide layer and partial reaction with the TBC material.

4. Conclusions

Rare earth doped NiCoCrAlY bond coats with 7YSZ TBCs on top have been examined on CMSX-4 substrates, both deposited by EB-PVD. A distinct lifetime prolongation was found for BCs with addition of Hf or Zr. Lifetimes of about 3000 cycles and more were reached at 1100°C, which corresponds to a tenfold increase in TBC lifetime compared to NiCoCrAlY-BC without RE co-doping.

The Hf doped bond coats show a longer lifetime with higher Hf content. The doping range of Hf with excellent results is relatively wide, ranging from 0.15 to 0.6 at.%. An excellent stability of HfO_2 that forms either islands for lower Hf contents or a continuous layer on top of the TGO was observed. The preferential diffusion path of RE elements along the alumina grain boundaries towards the TGO upper region could be determined via STEM investigations.

For Zr doping, the dependency of its concentration on the TBC lifetimes is different than that for Hf. Longer lifetimes were achieved with a low Zr content of 0.3 at.% while a higher doping content led to an increasing spinel formation with short lifetimes, i.e. no lifetime improvement in comparison to the undoped reference BC was found.

The microstructure of the TGO, its evolution with annealing time, and especially the incorporation of RE-oxides into the upper TGO zone seem to play a dominant role for TBC lifetime. While the total thickness of the TGO in the as coated stage increases with raising the RE-dopant concentration, the thickness of the alumina TGO layer decreases. Detailed TEM analyses revealed the presence of transient alumina and precipitation of RE particles within the TGO. During prolonged testing, spinel formation within the TGO did not reduce TBC life. Overall, Hf-doping seems to be more efficient than Zr-doping and it works over a wide range of doping level.

Acknowledgement

The authors express their gratitude to J. Brien, A. Handwerk, P. Herzog, and D. Peters (German Aerospace Center, Institute of Materials Research) for the technical support, coating manufacturing of the EB-PVD coatings and oxidation test processing. Additionally, the authors thank Peter Bauer and Frederic Kreps for preparing the FIB lamellae for TEM analysis. The TEM work was performed in the Framework of the Research Project 2016/23/G/ST5/04128, funded by National Science Centre, Poland.

Data availability

- The raw/processed data required to reproduce these findings cannot be shared at this time due to technical or time limitations.
- The raw/processed data required to reproduce these findings cannot be shared at this time as the data also forms part of an ongoing study.

References

1. Gleeson, B., *Thermal Barrier Coatings for Aeroengine Applications.* Journal of Propulsion and Power, 2006. **22**(2): p. 375-383.
2. Levi, C.G., *Emerging materials and processes for thermal barrier systems.* Current Opinion in Solid State & Materials Science, 2004. **8**: p. 77-91.
3. Schulz, U., et al., *Review on Advanced EB-PVD Ceramic Topcoats for TBC Applications.* International Journal of Applied Ceramic Technologies, 2004. **1**(4): p. 302-314.
4. Lehmann, H., et al., *Thermal Conductivity and Thermal Expansion Coefficients of the Lanthanum Rare-Earth-Element Zirconate System.* Journal of American Ceramic Society, 2003. **86**: p. 1338-1344.
5. Schulz, U., K. Fritscher, and A. Ebach-Stahl, *Cyclic behavior of EB-PVD thermal barrier coating systems with modified bond coats.* Surface and Coatings Technology, 2008. **203**: p. 449-455.
6. Munawar, A.U., et al. *Substrate Effect on the Lifetime of EB-PVD TBC Systems with 7YSZ and GDZ as ceramic top coat materials*. in *ASME Turbo Expo 2014*. 2014. Düsseldorf, Germany.
7. Meier Jackson, E.M., et al., *Effect of surface preparation on the durability of NiCoCrAlY coatings for oxidation protection and bond coats for thermal barrier coatings.* Materials and Corrosion, 2008. **59**(6): p. 494-500.
8. Yanar, N.M., F.S. Pettit, and G.H. Meier, *Failure Characteristics during Cyclic Oxidation of Yttria Stabilized Zirconia Thermal Barrier Coatings Deposited via Electron Beam Physical Vapor Deposition on Platinum Aluminide and on NiCoCrAlY Bond Coats with Processing Modifications for Improved Performances.* METALLURGICAL AND MATERIALS TRANSACTIONS A, 2006. **37**: p. 1563-1580.
9. Naumenko, D., et al., *Failure mechanisms of thermal barrier coatings on MCrAlY-type bondcoats associated with the formation of the thermally grown oxide.* Journal of Materials Science, 2009. **44**.
10. Subanovic, M., et al., *Effect of exposure conditions on the oxidation of MCrAlY-bondcoats and lifetime of thermal barrier coatings.* Surface and Coatings Technology, 2009. **204**: p. 820-823.
11. Soboyejo, W.O., et al., *High temperature oxidation interficial growth kinetics in YSZ thermal barrier coatings with bond coatings of NiCoCrAlY with 0.25%Hf.* Materials Science and Engineering A, 2011. **528**: p. 2223-2230.
12. Wei, L., et al., *Cyclic oxidation behavior of Hf/Zr co-doped EB-PVD β–NiAl coatings.* Surface and Coatings Technology, 2015. **276**: p. 4.
13. Haynes, J.A., et al., *Influence of Sulfur, Platinum, and Hafnium on the Oxidation Behavior of CVD NiAl Bond Coatings.* Oxidation of Metals, 2002. **58**(5/6): p. 513-544.
14. Padture, N.P., M. Gell, and E.H. Jordan, *Thermal Barrier Coatings for Gas-Turbine Engine Applications.* Science, 2002. **296**: p. 280-284.
15. Naumenko, D., et al., *Critical role of minor elemental constituents on the life time oxidation behaviour of FeCrAl-RE alloys.* EFC-Workshop "Life Time Modelling of High Temperature Corrosion Processes", Frankfurt, D, 22-23 February, 2001. Proceedings in European Federation of Corrosion Monograph, Nr. 34, Edts. M. Schütze, W.J. Quadakkers, J. Nicholls, The Institute of Materials, London, 2001, ISSN 1354-5116, 2001: p. 66-82.
16. Song, P., et al., *Effekt of atmosphere composition on the oxidation behavior of MCrAlY coatings.* Materials and Corrosion, 2011. **62**(No. 7): p. 699-705.
17. Heuer, A.H., et al., *Alumina Scale Formation: A New Perspective.* Journal of American Ceramic Society, 2011. **94**: p. 146-153.
18. Hou, P.Y., *Segregation Phenomena at Thermally Grown Al2O3/Alloy Interfaces.* Annu. Rev. Mater. Res., 2008. **38**: p. 275-298.
19. Pint, B.A., *Progress in Understanding the Reactive Element Effect Since the Whittle and Stringer Literature Review.* John Stringer Symp. High Temp. Corros. Mater. Park. ASM Int., 2003: p. 1-10.

20. Naumenko, D., B.A. Pint, and W.J. Quadakkers, *Current Thoughts on Reactive Element Effects in Alumina-Forming Systems: In Memory of John Stringer.* Oxidation of Metals, 2016. **86**: p. 1-43.
21. Hazel, B., et al., *Development of improved Bond Coat for enhanced turbine durability.* The Minerals/Metals and Materials Society, 2008: p. 753-760.
22. Munawar, A.U., U. Schulz, and M. Shahid, *Microstructure and lifetime of EB-PVD TBCs with Hf-doped bond coat and Gd-zirconate ceramic top coat on CMSX-4 substrate.* Surface and Coatings Technology, 2016. **299**: p. 104-112.
23. Murphy, K.S., K.L. More, and M.J. Lance, *As-deposited mixed zone in thermally grown oxide beneath a thermal barrier coating.* Surface and Coatings Technology, 2001. **146-147**: p. 152-161.
24. Levi, C.G., et al., *Alumina Grown during Deposition of Thermal Barrier Coatings on NiCrAlY.* Journal of American Ceramic Society, 2003. **86**(4): p. 676-685.
25. Braue, W., et al., *Nucleation and Growth of Oxide Constituents on NiCoCrAlY Bond Coats During the Different Stages of EB-PVD TBC Deposition and Upon Thermal Loading.* Materials Science Forum, 2004. **461-464**: p. 899-906.
26. Braue, W., et al. *Analytical electron microscopy of the mixed zone in NiCoCrAlY-based EB-PVD thermal barrier coatings: as-coated condition versus late stages of TBC lifetime*. in *Microscopy of oxidation*. 2005. Birmingham: Science Reviews.
27. Gil, A., et al., *Y-rich oxide distribution in plasma sprayed MCrAlY-coatings studied by SEM with a cathodoluminescence detector and Raman spectroscopy.* Surface and Coatings Technology, 2009. **204**: p. 531-538.
28. Vos, M., et al., *Oxygen Self-Diffusion in HfO2 Studied by Electron Spectroscopy.* Physical Review Letters, 2014. **112**.
29. Kilo, M., et al., *Oxygen diffusion in yttria stabilised zirconia—experimental results and molecular dynamics calculations.* Physical Chemistry Chemical Physics 2003. **5**: p. 2219-2224.
30. Nakagawa, T., et al., *Yttrium doping effect on oxygen grain boundary diffusion in a-Al2O3.* Acta Materialia, 2007. **55**: p. 6627-6633.
31. Schulz, U., et al., *Improvement of EB-PVD thermal barrier coatings by treatments of a vacuum plasma-sprayed bond coat.* Surface and Coatings Technology, 2008. **203**: p. 160-170.
32. Schulz, U., et al., *Influence of substrate material on oxidation behavior and cyclic lifetime of EB-PVD TBC systems.* Surface and Coatings Technology, 2001. **146-147**: p. 117-123.
33. Swadzba, R., *Interfacial phenomena and evolution of modified aluminide bondcoatings in Thermal Barrier Coatings.* Applied Surface Science, 2018. **445**: p. 133-144.
34. Swadzba, R., et al., *Microstructure degradation of EB-PVD TBCs on Pd–Pt-modified aluminide coatings under cyclic oxidation conditions.* Surface and Coatings Technology, 2013. **237**: p. 16-22.
35. Subanovic, M., et al., *Effect of manufacturing related parameters on oxidation properties of MCrAlY-bondcoats.* 2008. **59**(6): p. 463-470.
36. Quadakkers, W.J., et al., *THE SIGNIFICANCE OF BOND COAT OXIDATION FOR THE LIFE OF TBC COATINGS.* The Minerals, Metals & Materials Society, 1999: p. 119-130.
37. Ragan, D.D., T. Mates, and D.R. Clarke, *Effect of Yttrium and Erbium Ions on Epitaxial Phase Transformations in Alumina.* Journal of American Ceramic Society, 2003. **86**(4): p. 541-545.
38. Brickey, M.R. and J.L. Lee, *Structural and Chemical Analyses of a Thermally Grown Oxide Scale in Thermal Barrier Coatings Containing a Platinum–Nickel–Aluminide Bondcoat.* Oxidation of Metals, 2000. **54**(3-4): p. 237-254.
39. Pint, B.A. and K.L. More, *Characterization of alumina interfaces in TBC systems.* Journal of Materials Science, 2009. **44**: p. 1676–1686.
40. Pint, B.A. and K.A. Unocic, *Ionic segregation on grain boundaries in thermally grown alumina scales.* Materials at High Temperatures, 2012. **29**(3).
41. Unocic, K.A. and B.A. Pint, *Characterization of the alumina scale formed on a commercial MCrAlYHfSi coating.* Surface and Coatings Technology, 2010. **205**: p. 1178–1182.

42. Unocic, K.A., et al., *STEM and APT characterization of scale formation on a La,Hf,Ti-doped NiCrAl model alloy.* Micron, 2018. **109**: p. 41-52.
43. Whittle, D.P. and J. Stringer, *Improvement in properties: Additives in oxidation resistance.* Phil. Trans. R. Soc. Lond., 1980. **A 295**: p. 309-329.
44. Pint, B.A., *Experimental Observations in Support of the Dynamic-Segregation Theory to Explain the Reactive-Element Effect.* Oxidation of Metals, 1996. **45**(1/2): p. 1-37.
45. Swadzba, R., et al., *Characterization of Alumina Scales Grown on a 2nd Generation Single Crystal Ni Superalloy During Isothermal Oxidation at 1050, 1100 and 1150 C.* Oxidation of Metals, 2014. **82**: p. 195-208.
46. Rybicki, G.C. and J.L. Smialek, *Effect of the 0-a-A1203 Transformation on the Oxidation Behavior of/~-NiAI + Zr.* Oxidation of Metals, 1989. **31**(3/4): p. 275-304.
47. Pint, B.A., *On the Formation of Interfacial and Internal Voids in a-Al203 Scales.* Oxidation of Metals, 1997. **48**(3/4): p. 303-328.
48. Heuer, A.H., et al., *On the growth of Al2O3 scales.* Acta Materialia, 2013. **61**: p. 6670–6683.
49. Saldaña, J.M., et al., *Microstructure and lifetime of Hf or Zr doped sputtered NiAlCr bond coat/7YSZ EB-PVD TBC systems.* Surface and Coatings Technology, 2018. **335**: p. 41-51.

Figure captions

Fig. 1: SEM micrograph of the as coated state of the reference NiCoCrAlY coating system (without co-doping).

Fig. 2: SEM micrograph of the as coated state, a) 0.3Hf-BC and b) 0.6Hf-BC.

Fig. 3: a, b) STEM-HAADF image of the YSZ / TGO of 0.3Hf-BC in the as coated state, c) electron diffraction for HfO_2 and d-h) elemental mapping in the window marked in Fig. 3b.

Fig. 4: STEM-HAADF image (a) of the mixed zone in TGO formed on the 0.3Hf-BC and b) HRTEM image along with electron diffraction containing γ- and θ-Al_2O_3 along with tetragonal ZrO_2.

Fig. 5: SEM micrograph of the as coated state, a) 0.3Zr-BC, b) 0.7Zr-BC and c) 1.0Zr-BC.

Fig. 6: TGO thickness in the as coated state of all variants investigated plotted over the content of doping element.

Fig. 7: Schematic representation of formation process of a TGO microstructure on NiCoCrAlY bond coats, valid for Hf- and Zr-doped coatings after TBC deposition (described in [26]).

Fig. 8: Cyclic lifetimes of 7YSZ TBCs at 1100°C on various co-doped bond coats in comparison to reference (data from [5]). The insert shows an exemplary macroscopic picture of a 0.3 at.% Hf doped sample after 3450 cycles.

Fig. 9: Lifetime in cycles as a function of doping content in at.%.

Fig. 10: SEM micrographs of Hf-doped NiCoCrAlY coating systems after failure at 1100°C cycle test, a) 0.15Hf-BC after 2929 cycles and b, c) 0.3Hf-BC after 3146 cycles.

Fig. 11. STEM-HAADF (a) and b) STEM-ADF images of the YSZ / TGO interface on the 0.3Hf-BC after 3450 cycles at 1100°C test.

Fig. 12: STEM-HAADF images of the TGO formed during the 1100°C cyclic oxidation testing for 3450cycles on the 0.3Hf-BC along with elemental mapping (c-j) and electron diffraction patterns for k) HfO_2, l) $NiAl_2O_4$ and m) Y_2O_3.

Fig. 13: STEM-HAADF images of the α-Al_2O_3 grain boundaries in the TGO formed during the 1100°C cyclic oxidation testing for 3450cycles on the 0.3Hf-BC along with elemental mapping of the reactive elements: c) Hf, d) Y, e) Zr along with f) Ni, g) Al and h) O.

Fig. 14: SEM micrographs of Zr-doped coating systems after failure at 1100°C cycle test, a) 0.7Zr-BC after 664 cycles and b) 0.3Zr-BC after 2790 cycles.

Tables

Table 1: Composition of NiCoCrAlY bond coats and substrate material; data in at.%

	Ni	Co	Cr	Al	Y	Hf	Zr	other
Reference	39-40	19	18-19	22	0.07-0.11	-	-	-
Hf-doped	40-41	18-19	17-18.5	23	0.1-0.2	0.05, 0.15, 0.3 or 0.6	-	-
Zr-doped	40-41	18-19	17-18.5	23	0.1-0.2	-	0.3, 0.7, or 1.0	-
CMSX-4	64	9	7.5	12.5	-	0.03	-	2 Ta, 2 W, 1.3Ti, 1 Re, 0.4 Mo

Figures

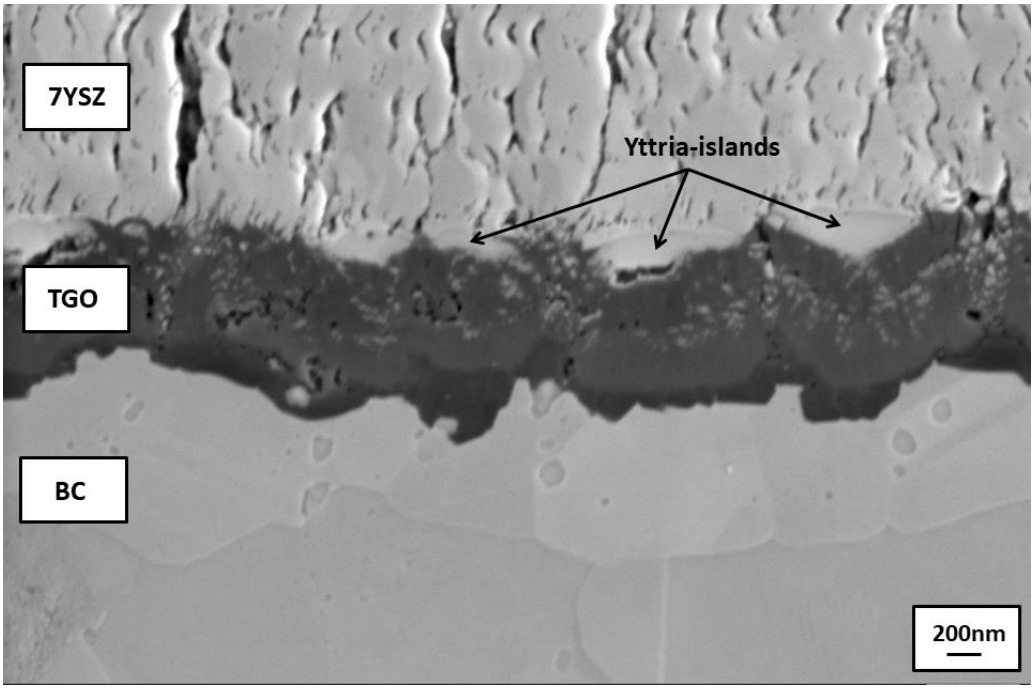

Fig. 1

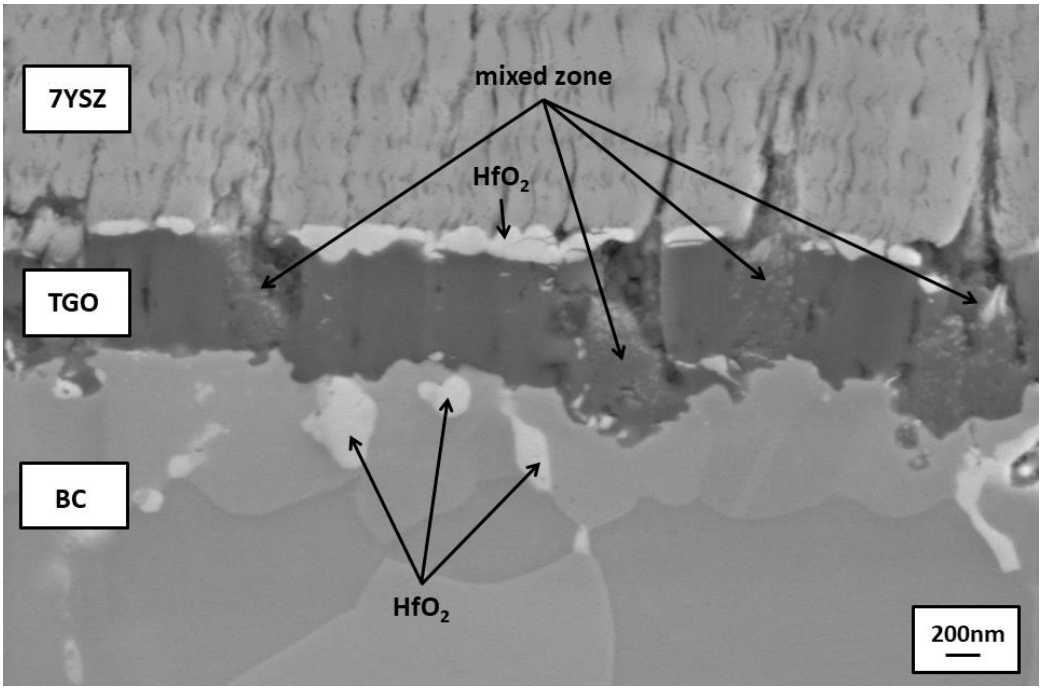

Fig. 2 a)

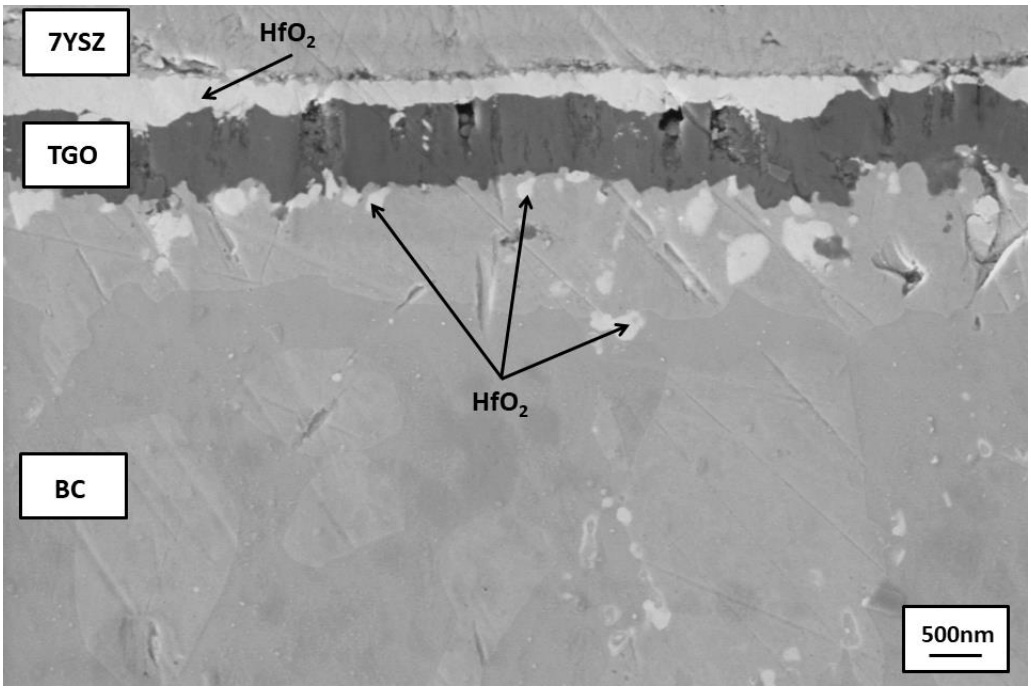

Fig.2b)

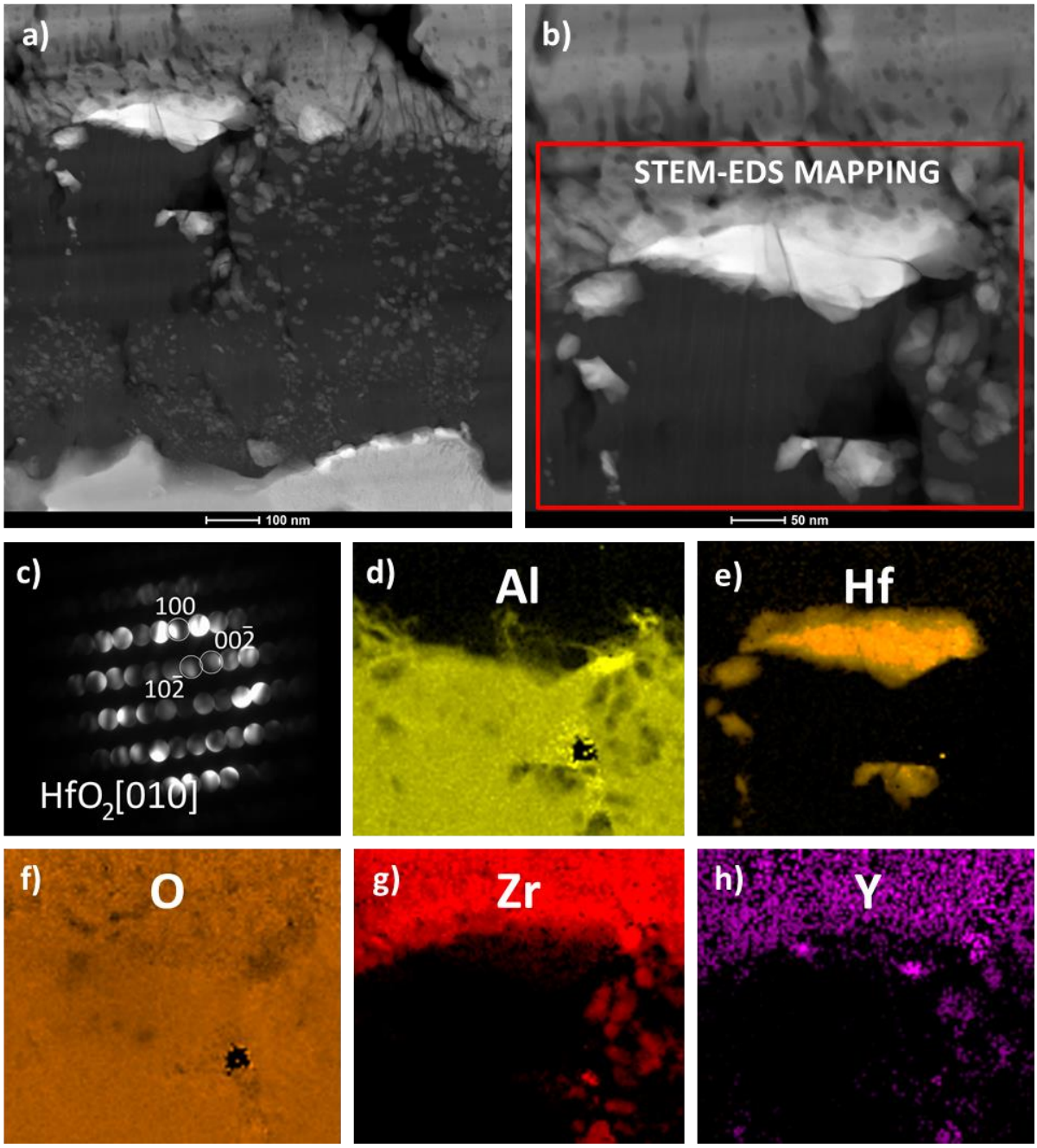
a)
100 nm
b)
STEM-EDS MAPPING
50 nm
c)
100
002̄
102̄
HfO2[010]
d)
Al
e)
Hf
f)
O
g)
Zr
h)
Y

Figure 3

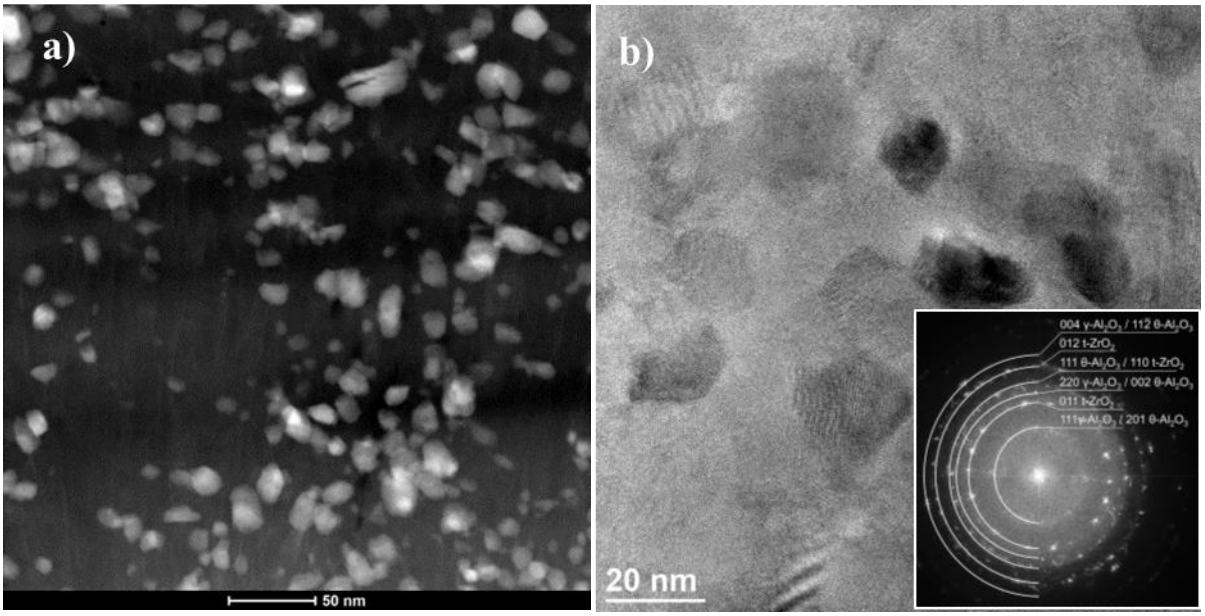

Figure 4

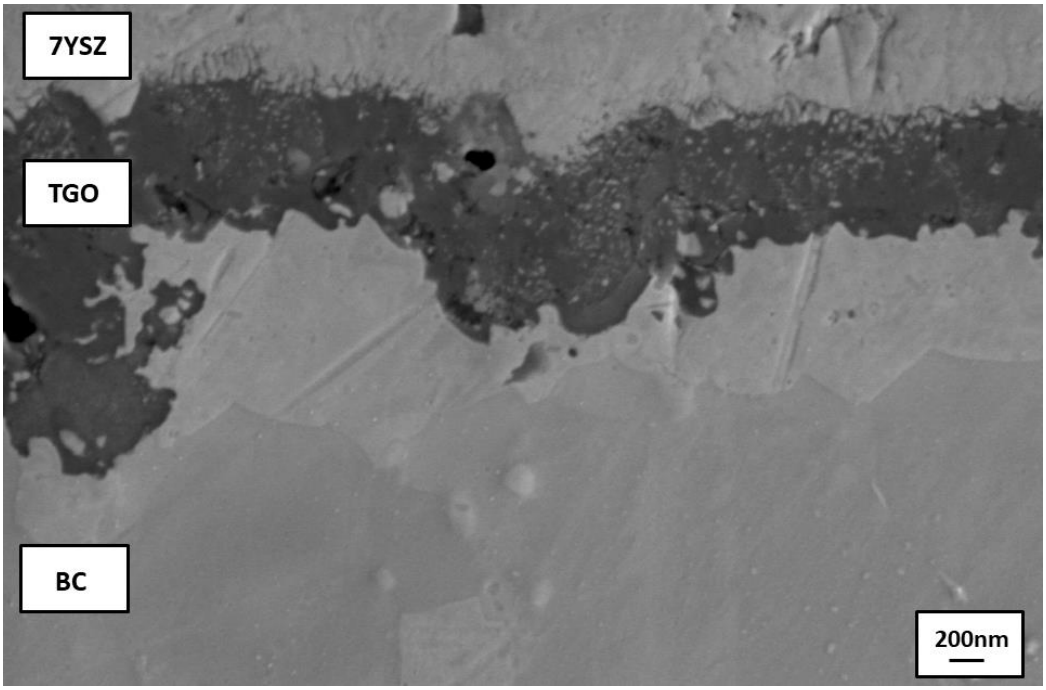

Fig. 5a

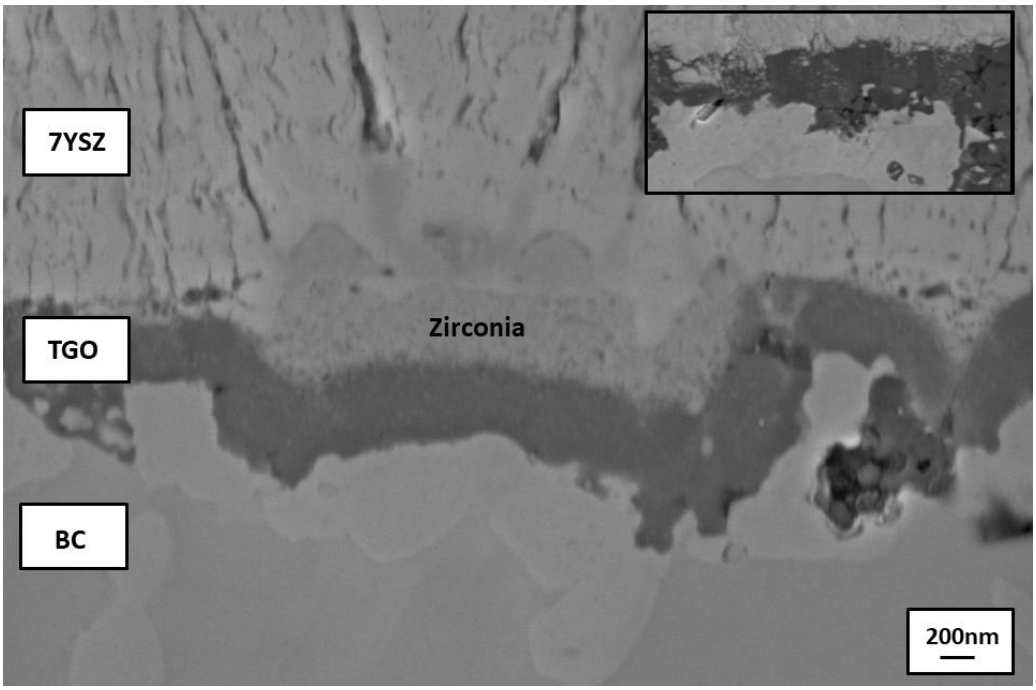

Fig. 5b)

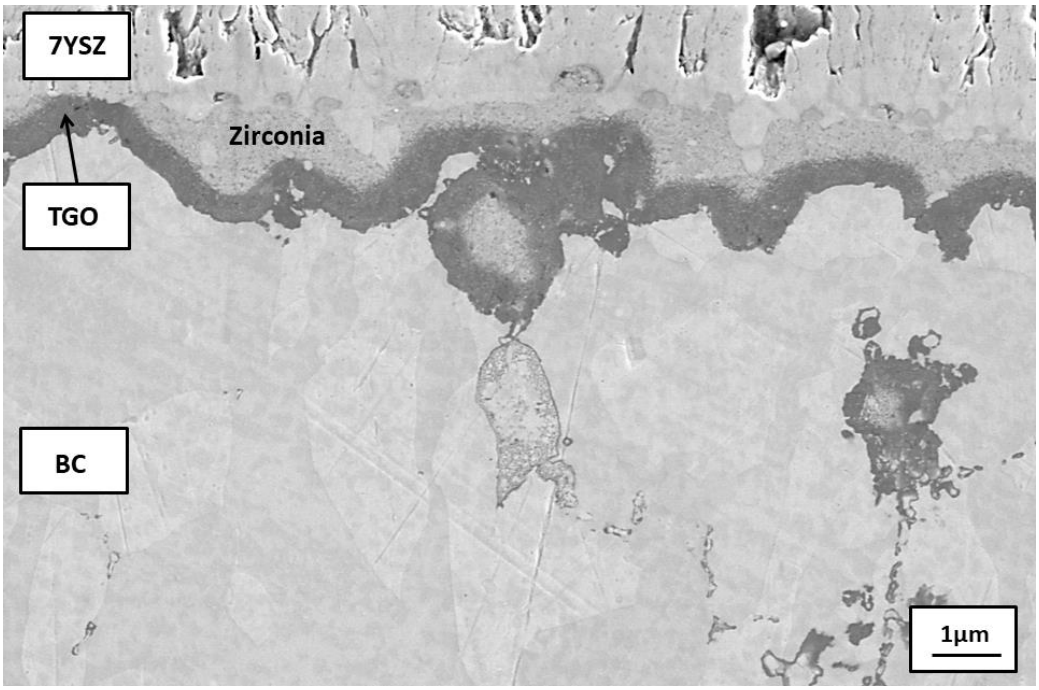

Fig. 5c)

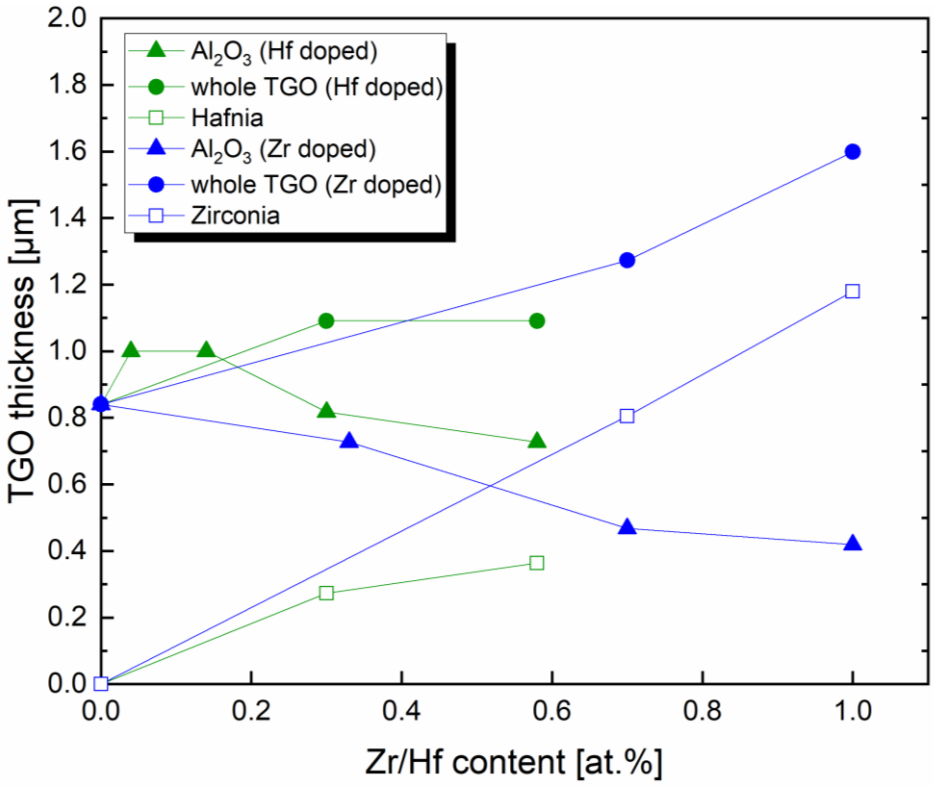
Al2O3 (Hf doped)
whole TGO (Hf doped)
Hafnia
Al2O3 (Zr doped)
whole TGO (Zr doped)
Zirconia
TGO thickness [µm]
Zr/Hf content [at.%]
0.0
0.2
0.4
0.6
0.8
1.0
1.2
1.4
1.6
1.8
2.0

Fig. 6

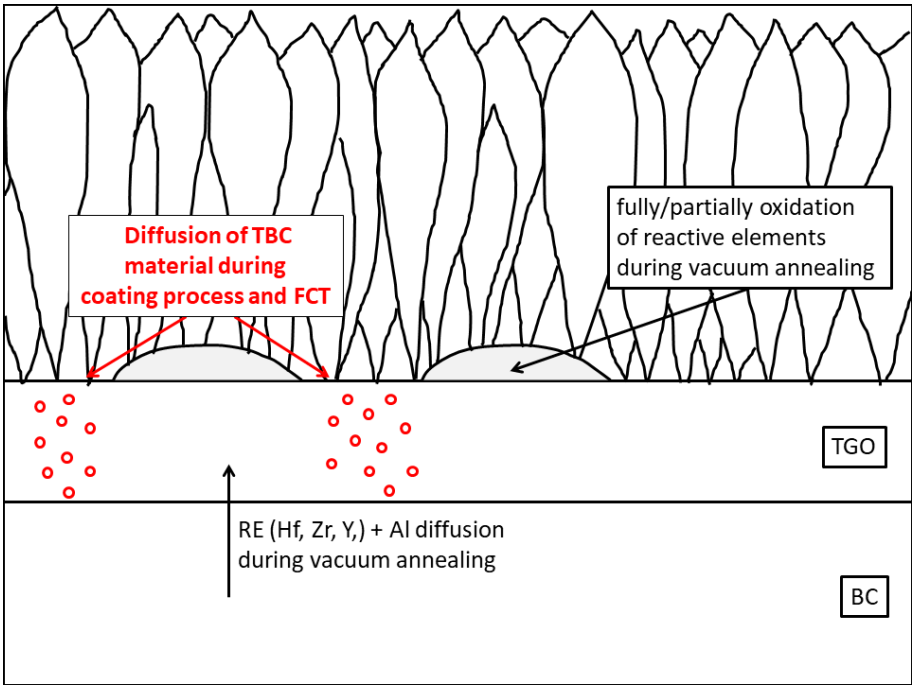
Diffusion of TBC material during coating process and FCT
fully/partially oxidation of reactive elements during vacuum annealing
TGO
RE (Hf, Zr, Y,) + Al diffusion during vacuum annealing
BC

Fig. 7

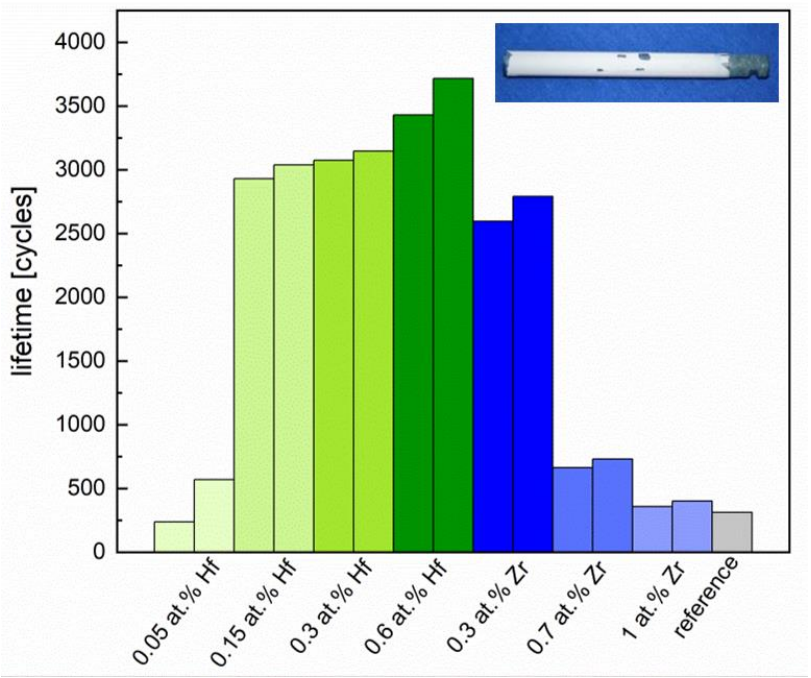
lifetime [cycles]
4000
3500
3000
2500
2000
1500
1000
500
0
0.05 at.% Hf
0.15 at.% Hf
0.3 at.% Hf
0.6 at.% Hf
0.3 at.% Zr
0.7 at.% Zr
1 at.% Zr
reference

Fig. 8

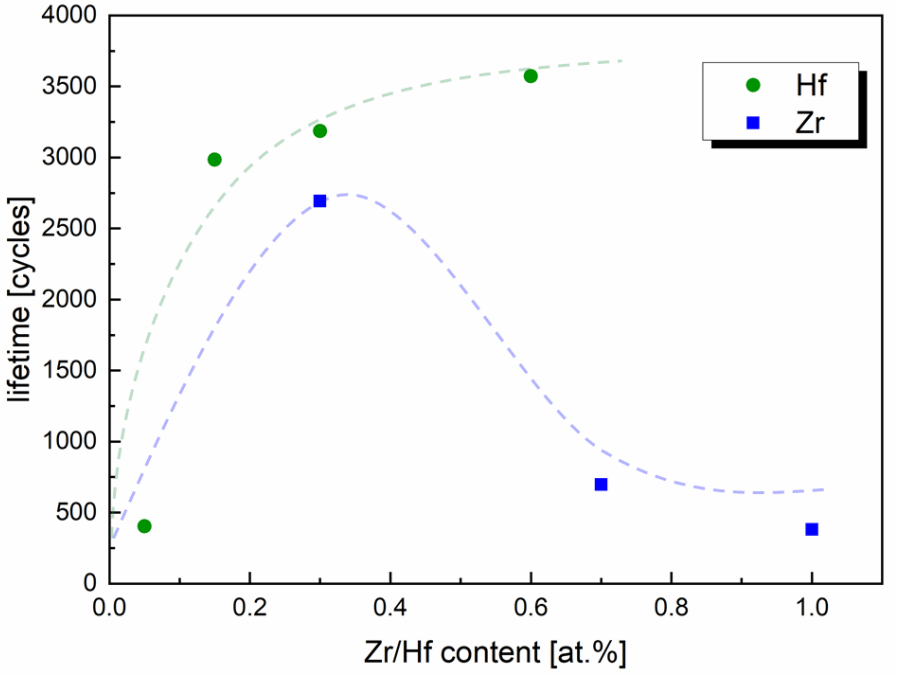
lifetime [cycles]
4000
3500
3000
2500
2000
1500
1000
500
0
0.0
0.2
0.4
0.6
0.8
1.0
Zr/Hf content [at.%]
Hf
Zr

Fig. 9

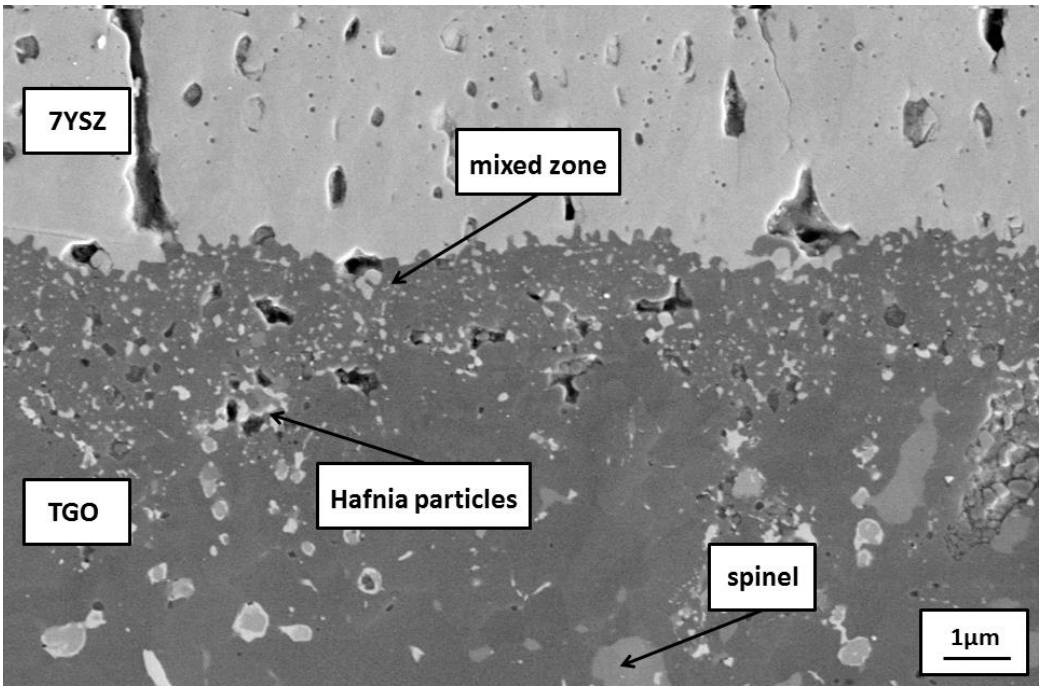

Fig. 10a)

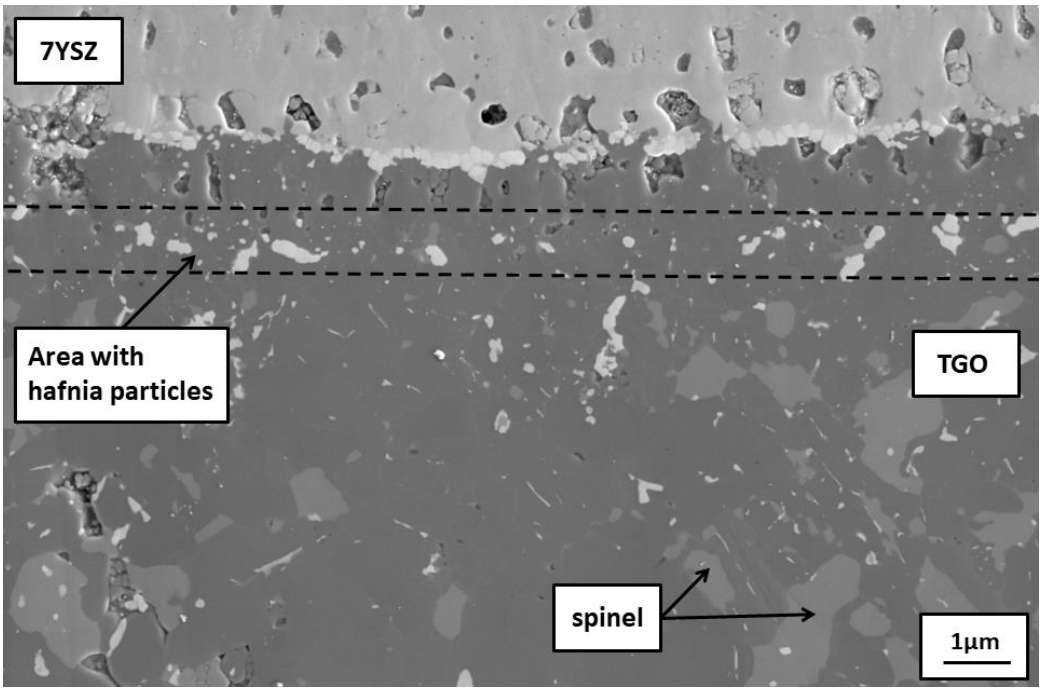

Fig. 10b)

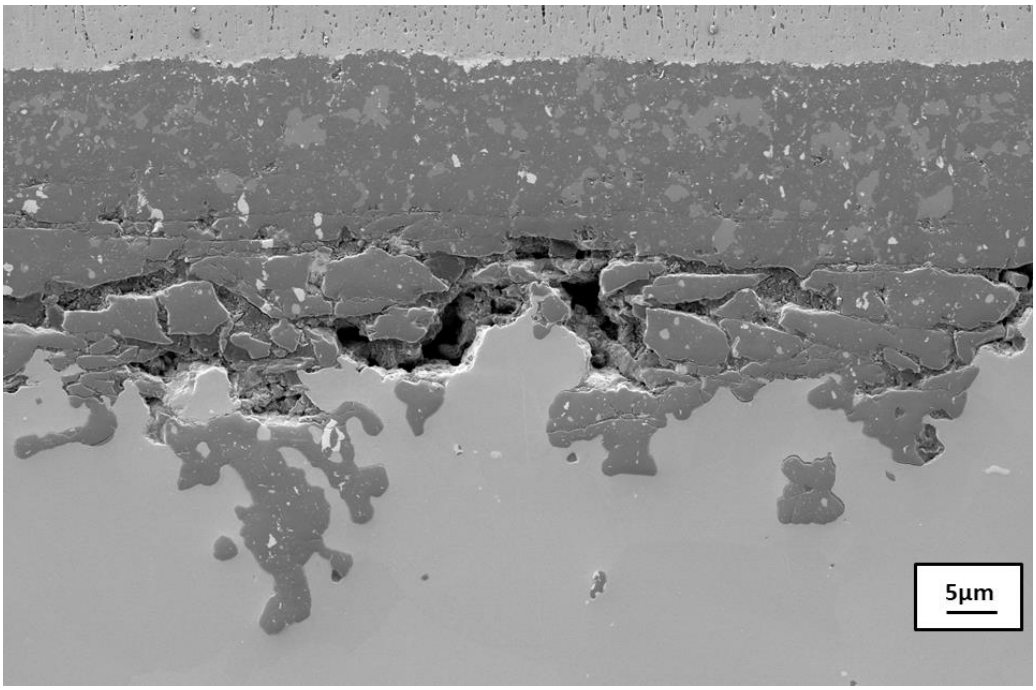

Fig. 10c)

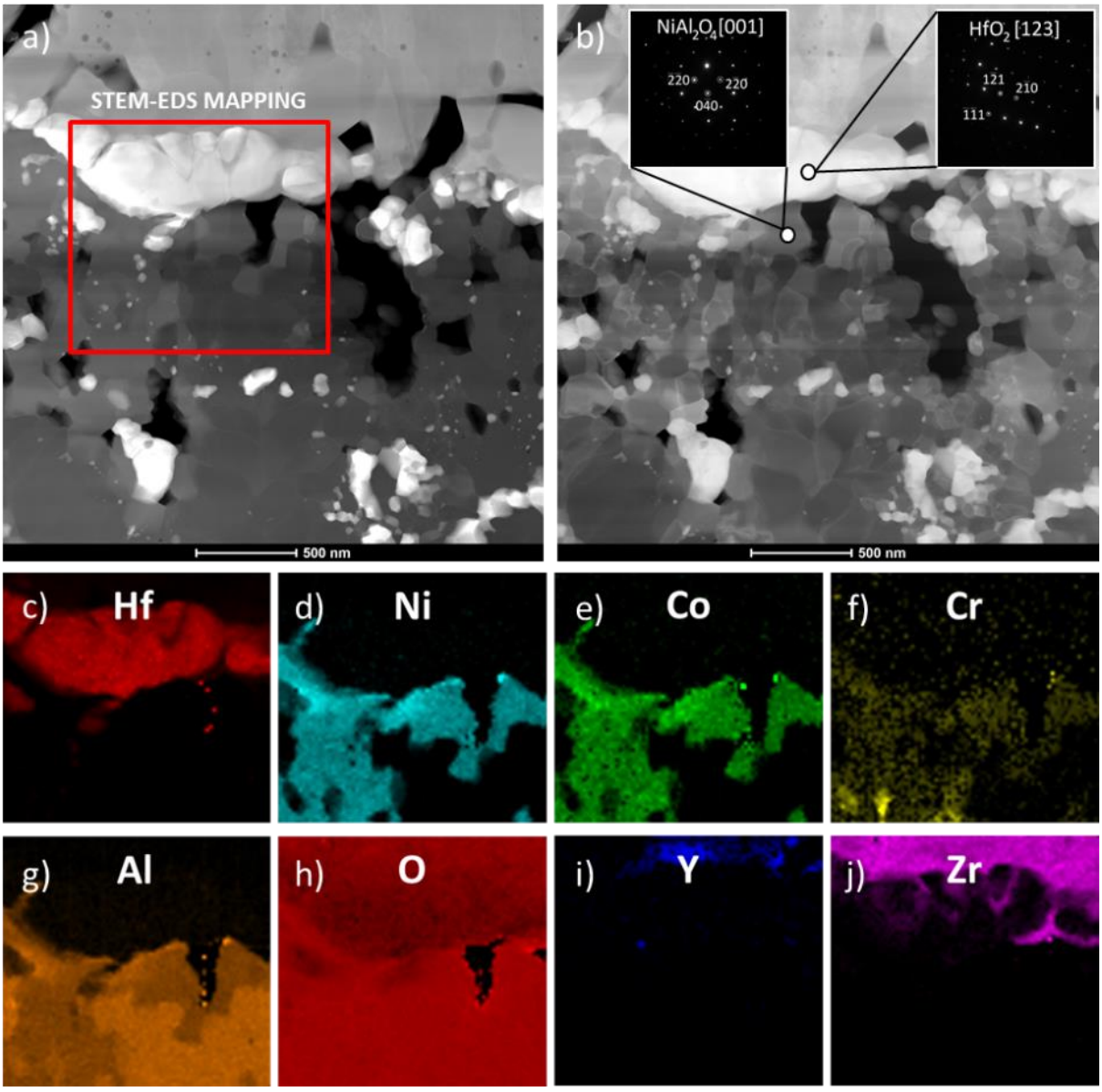
a)
STEM-EDS MAPPING
500 nm
b)
NiAl2O4 [001]
220
220
040
HfO2 [123]
121
210
111
500 nm
c) Hf
d) Ni
e) Co
f) Cr
g) Al
h) O
i) Y
j) Zr

Figure 11

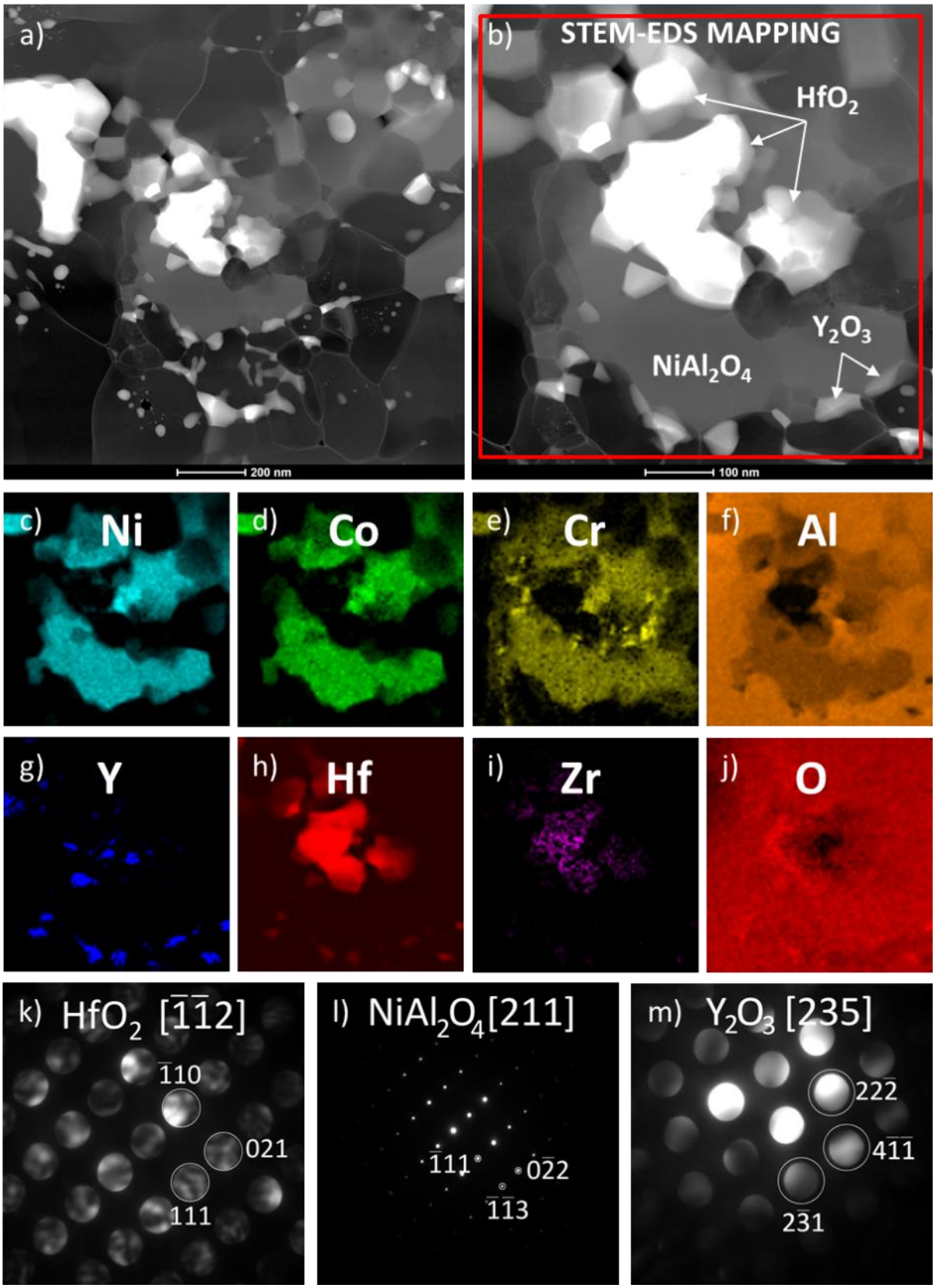
a)
200 nm
b) STEM-EDS MAPPING
HfO_2
Y_2O_3
$NiAl_2O_4$
100 nm
c) Ni
d) Co
e) Cr
f) Al
g) Y
h) Hf
i) Zr
j) O
k) HfO_2 [$\bar{1}\bar{1}2$]
$\bar{1}10$
021
111
l) $NiAl_2O_4$[211]
$\bar{1}11$
$0\bar{2}2$
$\bar{1}\bar{1}3$
m) Y_2O_3 [235]
$22\bar{2}$
$4\bar{1}\bar{1}$
$2\bar{3}1$

Figure 12

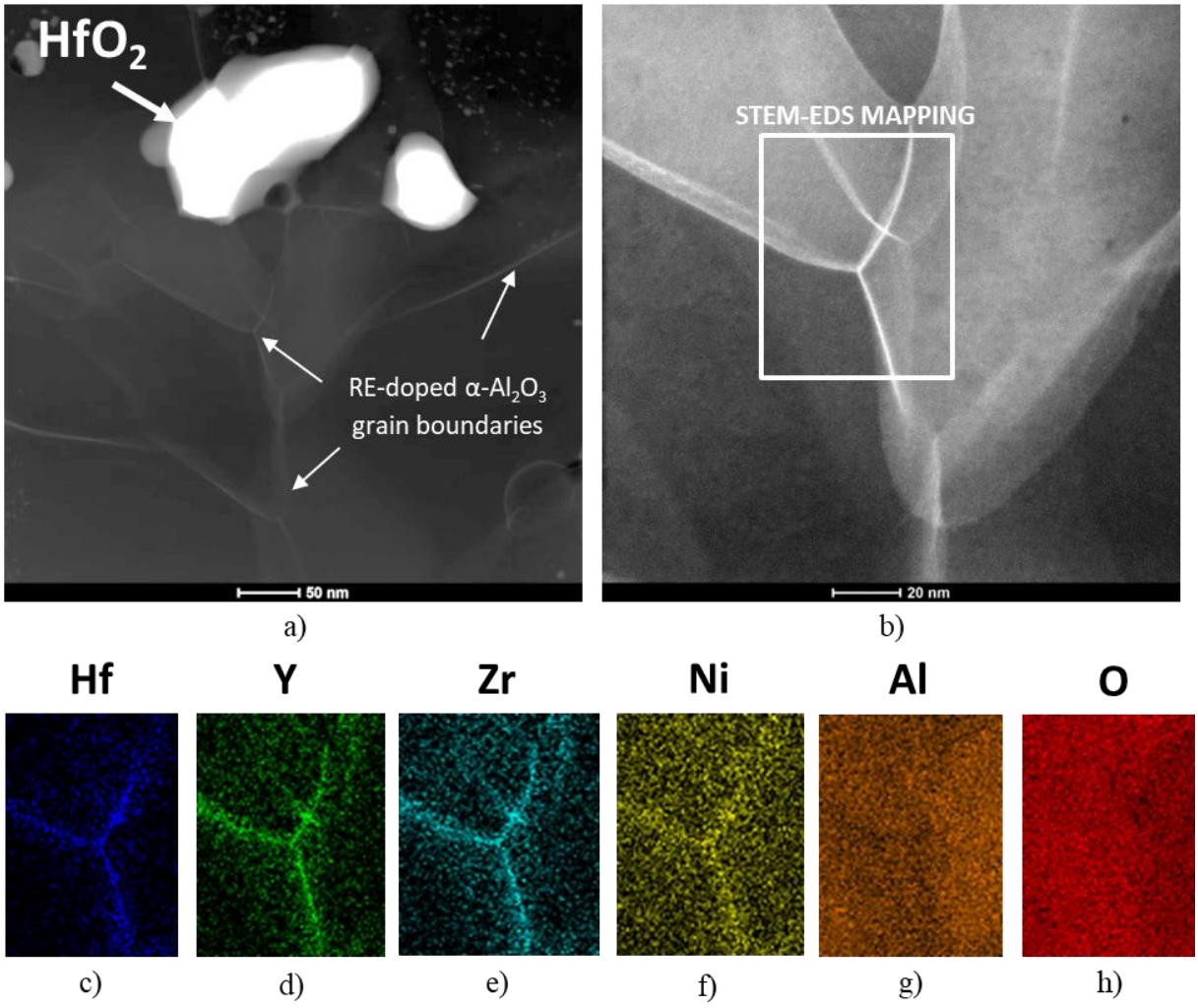
HfO2
RE-doped α-Al2O3
grain boundaries
50 nm
STEM-EDS MAPPING
20 nm
a)
b)
Hf
Y
Zr
Ni
Al
O
c)
d)
e)
f)
g)
h)

Figure 13

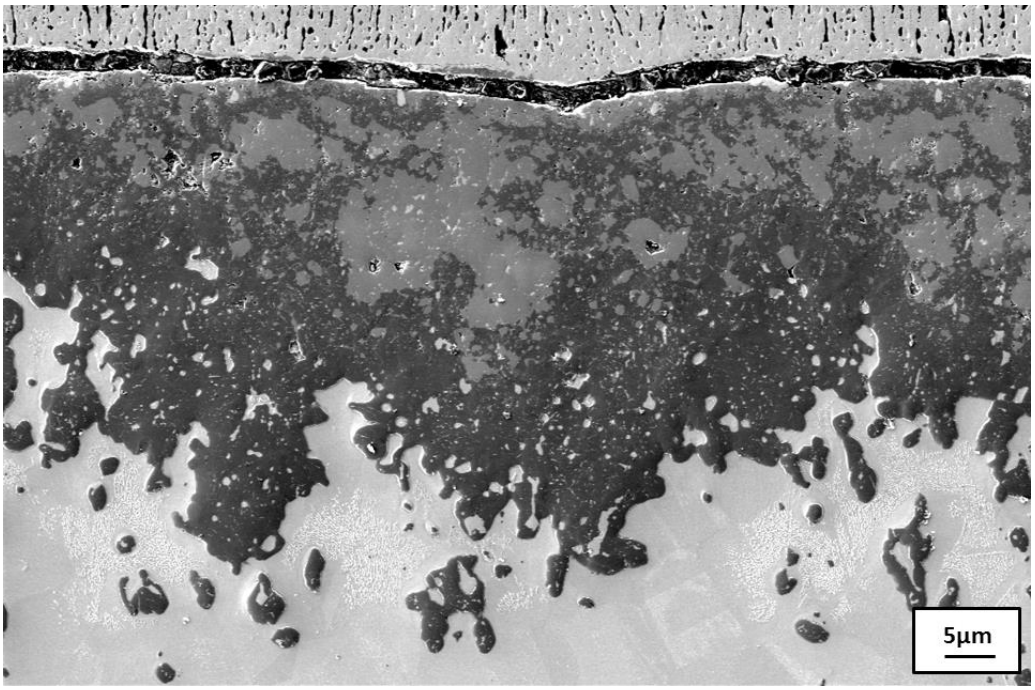

Fig. 14a)

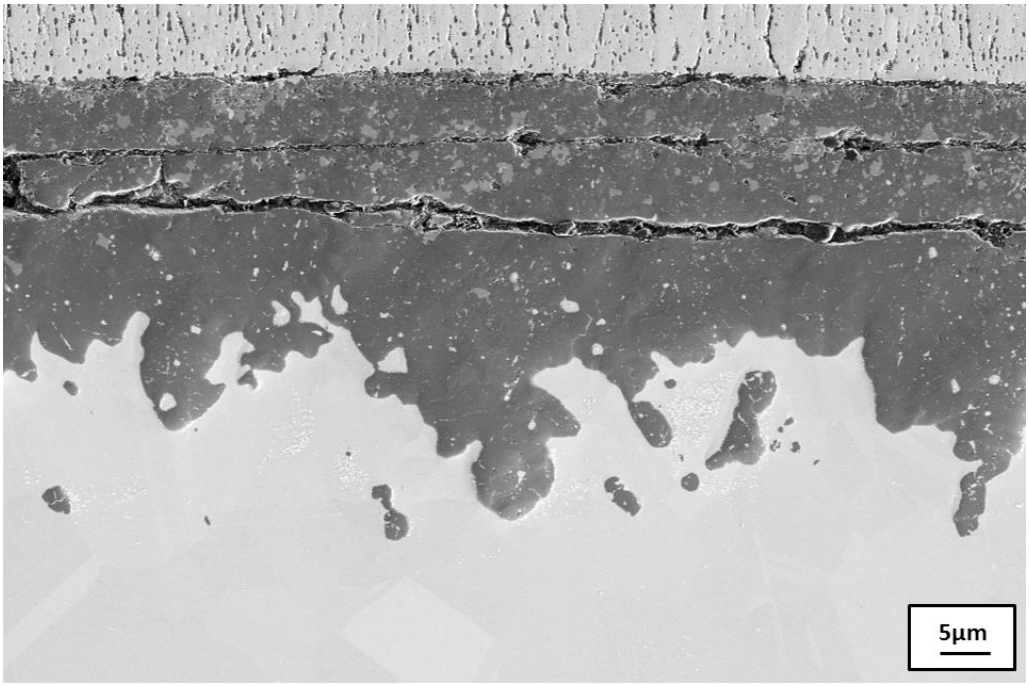

Fig. 14b)